Accepted manuscript doi:
10.1680/jgeot.16.p.325

Submitted: 13 December 2016

Published online in 'accepted manuscript' format: 07 November 2018

Manuscript title: Rigid pile response to cyclic lateral loading: laboratory tests

Authors: Christelle N. Abadie*, Byron W. Byrne† and Guy T. Houlsby†

Affiliations: *Department of Engineering, University of Cambridge, Cambridge, UK (formerly Department of Engineering Science, University of Oxford) and †Department of Engineering Science, University of Oxford, Oxford, UK

Corresponding author: Christelle N. Abadie, University of Cambridge, Department of Engineering, Trumpington Street, Cambridge CB2 1PZ, UK. Tel.: +44 1223 3 30278.

E-mail: cna24@cam.ac.uk

Accepted manuscript doi:
10.1680/jgeot.16.p.325

Abstract

This paper presents experimental work aimed at improving understanding of the behaviour of rigid monopiles, in cohesionless soils, subjected to lateral cyclic loading. It involves 1-g laboratory model tests, scaled to represent monopile foundations for offshore wind-turbines. The test programme is designed to identify the key mechanisms governing pile response, and is divided into four main parts: (i) investigation of loading rate effects, (ii) hysteretic behaviour during unloading and reloading, (iii) pile response due to long-term single amplitude cyclic loading and (iv) multi-amplitude cyclic loads. The results show that the pile response conforms closely to the extended Masing rules, with additional permanent deformation accumulated during non-symmetric cyclic loads. This ratcheting behaviour is characterised by two features: first, the ratcheting rate decreases with cycle number and depends on the cyclic load magnitude and secondly, the shape of the hysteresis loop tightens progressively, involving increased secant stiffness and decreased loop area. Test results involving multi-amplitude load scenarios demonstrate that the response of the pile to complex load scenarios can be analysed and understood using the conclusions from single amplitude cyclic loading. Such test results should be sufficient for deriving the principles of new modelling approaches.

Keywords: Laboratory tests; Offshore engineering; Piles; Plasticity; Repeated loading; Sands; Stiffness

Accepted manuscript doi:
10.1680/jgeot.16.p.325

Introduction

Offshore wind plays an important role in the transition to low carbon energy supply, and has developed rapidly over the past decade, particularly in Europe. Most offshore wind turbines are founded on single large diameter piles, called monopiles. The design is simple, cost-effective and robust in most soil conditions. It is well suited to many current and future projects. In comparison, other foundation systems (e.g. multi-piled foundations requiring jackets) are usually more expensive and complicated to design, mass-produce, transport and install. Accordingly, there is significant momentum in the offshore wind industry to further the understanding and optimization of monopile design to: (i) reduce their weight, (ii) allows them to be used in deeper water to displace jacket type structures, (iii) extend their service life and (iv) make them suitable for larger turbines.

The anticipated lifetime of an offshore wind structure is nominally 20 to 25 years (EWEA, 2009), during which the monopile is subjected to many different loading conditions. The design must account for the ultimate load conditions, and recent work has made significant advances in this area (e.g. Byrne et al., 2015). One of the key areas of uncertainty, however, involves accounting for the effects of cyclic loading, particularly on the structural integrity of the turbine. The fundamental mode of vibration of the structure is a function of the foundation stiffness, and assessing any evolution of this stiffness with time is vital for accurate estimation of the fatigue life. In addition, the amplitude of the structural vibrations are governed by the damping of the foundation-structure system, which strongly depends on soil damping (e.g. Germanischer Lloyd, 2005). For large diameter monopiles, total soil damping is likely to be governed by material damping, which is derived from the hysteretic response of the pile-soil response, corresponding to dissipation of energy by the soil being loaded and unloaded (Cook and Vandiver, 1982, Tarp-Johansen et al., 2009). Finally, a robust design must ensure limited displacement of the structure and foundation over time to meet serviceability requirements, with the maximum tilt of the support structure generally specified by turbine manufacturers to guarantee good operation of the turbine (e.g. DNV, 2016, Section 7.6.2.7, p. 123). Therefore, serviceability and fatigue designs of the foundation are driven by (i) an accurate prediction of the evolution of permanent deformations, (ii) foundation stiffness, both during extreme events and operational conditions, and, (iii) determination of the foundation hysteretic damping.

Regrettably, the pile response due to lateral cyclic loading, and assessment of the three criteria listed above, are poorly accounted for in current design practice, such as in the *p-y* methods (e.g. API, 2010, DNV, 2016). A better understanding of the foundation behaviour, leading to updated guidelines, is needed if efficiencies are to be gained. This has motivated a number of research projects. For example, empirical laws describing the evolution of pile rotation and stiffness with the number of cycles, during both continuous and multi-amplitude loading conditions, have been recently derived based on experimental work (e.g. LeBlanc et al., 2010b, Peralta, 2010, Klinkvort, 2012, Cuéllar, 2011, LeBlanc et al., 2010a). Such approaches can be readily integrated into current design approaches, and provide an acceptable first approximation to pile behaviour (Abadie, 2015). However, these procedures are highly empirical and do not provide detailed (cycle by cycle) information on the plastic response, nor insight into the damping derived from the foundation element. They are also unable to predict the pile response following cyclic loading, and hence, any potential change in the Ultimate Limit State (ULS). There is a need for more rigorous approaches to describe the cyclic behaviour and the mechanisms of the soil response.

To address the above limitations this paper describes laboratory scale testing, focused on a rigid pile embedded in a cohesionless soil (dry sand). The experimental work is directed towards analysis of the plastic response and identification of the key mechanisms driving the global pile response during cyclic quasi-static loading of relatively small magnitude and low frequencies, similar to wave loading. The work provides impetus for development of new constitutive models, which can accurately capture pile response to cyclic lateral loading (both continuous and multi-amplitude). The limitations of the experimental programme presented here (small scale, dry sand, limited number of cycles) should of course be properly recognised when applying the results to full scale design.

Accepted manuscript doi:
10.1680/jgeot.16.p.325

Experimental methods

Scaling considerations

The results presented here were derived using 1-g laboratory floor model tests. The main focus of the work was to explore phenomenological behaviour for building of theoretical models, rather than a response targeted at a specific site. However, scaling was considered carefully to ensure the responses observed were representative of field problems. The dimensionless framework adopted for this experimental study followed that of LeBlanc et al. (2010a,b), as shown in Table 1. The earlier work of Bolton (1986), elaborated further in LeBlanc et al. (2010b), highlights the importance of scaling of sample properties for 1g model testing, particularly, the sample relative density in the laboratory must be reduced to be representative of the soil dilatancy at full scale (Byrne and Houlsby, 2004). In addition, consideration is also given to the pile aspect ratio (embedded length over diameter, L/D) and pile relative stiffness (K_R), following observations from Dietrich (1982) and Peralta (2010). The pile relative stiffness is calculated according to Poulos (1982):

$$K_R = \frac{E_p I_p}{E_{SL} \cdot L^4} \quad \begin{cases} > 0.208 & \textit{Rigid pile} \\ < 0.0025 & \textit{Slender pile} \end{cases} \tag{1}$$

E_pI_p is the pile bending stiffness and E_{SL} is the soil Young's modulus at the pile tip, estimated from the small strain shear modulus ($E_{SL}=2(1+\nu)G_0$). Fig. 1 shows aspect ratio plotted against pile relative stiffness for a range of designs relevant to UK offshore wind farms (OWF). Three sets of data are highlighted: (i) current wind farm monopiles in sand, (ii) current wind farm monopiles in clay and (iii) piles used in the 1960s and 1970s for development of current *p-y* methods (e.g. API, 2010, DNV, 2016). Fig. 1 identifies the region where model piles would capture field monopile conditions; these values were adopted in the tests described below.

Testing equipment

The model experiments were conducted using equipment developed by Rovere (2004), and used further by LeBlanc et al. (2010a,b). Fig. 2 shows the system, which consists of a combination of rotating and suspended masses, a motor, a steel support structure and a sand container. The motor and the main beam, which pivots about a horizontal axis, are balanced by the mass m_3. Continuous loading is achieved using the motor to drive the rotating mass, with m_1 and m_2 selected to achieve the appropriate load on the pile. The motor frequency is set at 0.106 Hz. This corresponds to the peak frequency of offshore waves and is sufficiently low to avoid dynamic effects from the soil response. The rig can also be used to perform incremental loading, or creep, tests. This is achieved by hanging masses successively on the relevant side of the pile (the motor is not used). This testing technique enables accurate 2-way loading to be applied to the pile and can be used to assess the influence of rate on the pile response.

The samples were prepared in a 600 mm x 600 mm x 527 mm tank, with sufficient clearance between pile and container wall to avoid significant boundary effects. The sand was poured from a low drop height to achieve a very low relative density, allowing for very repeatable and reliable sample preparation. The low relative density minimised the effect of soil dilation, corresponding to higher densities in the field where the stresses are much greater. All samples were prepared dry to allow for drained conditions and used Yellow D14/25 Leighton Buzzard sand (Table 2). The relative densities of the samples were deduced by weight of sand introduced to the tank. The average sample weight was 284 ± 2 kg, leading to sample average relative densities of 2%. The tests were performed using a stiff copper pile (Table 3), of which the outer dimensions were scaled to 1:80 of a typical 3.6 MW turbine monopile. However, it is also geometrically similar to larger or smaller wind turbine monopiles. During installation, the pile was fixed horizontally, and driven into the sand sample using a rubber hammer. When it reaches the final penetration depth, the number of hammer strokes and the

sand plug depth inside the pile were compared, with high consistency between tests. The horizontal load was applied at a relevant fixed height above the sand bed surface (Table 3).
High-quality continuous measurement of the pile deflection was obtained using two DC RDP electronic Linear Variable Differential Transformers (LVDTs). The pile rotation was also calculated. The load applied to the pile head was monitored using a load-cell. The instrumentation used during this research programme captured accurately the macro-behaviour of the pile, i.e. the horizontal force applied, the displacement at ground level, the rotation, and the parameters that can be derived from these macro variables (moment at ground level, tangent and secant stiffness and dissipated energy in particular). The macro-behaviour was the focus of theoretical developments as described in Abadie (2015) and Houlsby et al. (2017).

Test programme

The testing initially involved (Phase 1) monotonic loading tests to provide the static pile load-displacement response, also known as the *backbone curve*, and, (Phase 2) tests focused on symmetric reversed loading to provide the primary hysteretic response. This second set of tests highlighted the importance of the initial loading curve in the determination of the subsequent cyclic loading response. The framework was then extended to (Phase 3) long-term non-symmetric continuous cyclic loads, targeting evolutions of (a) the pile deformation (b) the secant stiffness and (c) the hysteretic damping (measured as the hysteresis loop area). In addition, the cyclic tests performed were followed by monotonic loading to provide insight into the evolution of pile capacity following cyclic loading. Finally, the framework was developed further with (Phase 4) tests directed towards pile response to multi-amplitude loading, targeting the effect of alternating storm-type events with continuous operational loads. The detailed test program is shown in Table 4. For the cyclic loading tests the loading is characterized by two normalising parameters: the magnitude ζ_b and amplitude ζ_c (LeBlanc et al., 2010b).

$$\zeta_b = \frac{M_{\max}}{M_R} \tag{2}$$

$$\zeta_c = \frac{M_{\min}}{M_{\max}} \tag{3}$$

where M_{min} and M_{max} are the minimum and maximum moment over a load cycle and M_R is the static moment capacity of the pile. The values of ζ_b and ζ_c for the continuous and multi-amplitude cyclic test have been chosen according to the design limit states specified in LeBlanc et al. (2010b). For the creep tests, the load step was 0.5 kg and the incremental time step is indicated within brackets, with "3/1 min" defined as 3 minute time-steps during loading and 1 minute time steps during unloading. The continuous cyclic tests followed by a monotonic test are referred to as "Continuous+Monotonic". The details for Phase 4 multi-amplitude loading is provided in Table 5.

Validation of testing techniques

Fig. 3 shows the monotonic tests MCo and MCo1-3 demonstrating the high repeatability obtained in the experimental work. Similar precision was also obtained when comparing the data of analogous incremental tests. Significant confidence can therefore be attached to the conclusions drawn from comparison of different tests.
Further validation of the testing equipment and modelling choices (e.g. the stress level at 1-g, low relative density) was achieved by comparison of the test results with relevant tests from the published literature. The selected tests (Table 6) involved a range of load eccentricities, pile geometries, sand densities and testing procedures in the laboratory (1-g and centrifuge), as well as data from field testing on a large scale monopile in sand (PISA Project at Dunkirk site, Burd et al., 2017). To limit the error arising from post-processing of the data from the literature, the results are converted to moment load - displacement space and normalised using the moment at the defined ultimate capacity

Accepted manuscript doi:
10.1680/jgeot.16.p.325

and pile diameter. The results are shown in Fig. 4, demonstrating that the pile response obtained in the experimental work compares well with the framework currently observed for stiff piles in cohesionless soils.

Monotonic test results

Ultimate capacity and initial stiffness

The ultimate capacity of the pile, M_R, provides a reference value for choice of load magnitudes in the cyclic loading tests. There is little guidance from design standards concerning the appropriate definition of pile failure, and no clear failure point appears on typical moment-rotation (or load-displacement) curves. A maximum tolerance for pile deformation is usually specified by the turbine manufacturer (DNV, 2016, p. 123). Byrne et al. (2015) propose an ultimate criterion defined by the minimum moment at either a ground level displacement of υ_R=10% x D or a ground level rotation of θ_R=2 degrees. This criterion was applied to test MCo (Fig. 3) with the limiting value given as $\tilde{M}_R = 0.63$ or M_R=33.5 Nm. The small range of the LVDTs required the limiting value to be extrapolated from a fit to the measured results. The monotonic test results also enabled determination of the initial modulus E_0 of the pile-soil interaction (tangent to the origin of the moment-rotation curve), later used as a reference value for the evolution of the cyclic tangent shear modulus. The results from test MCo give E_0= 65 kNm.rad^{-1}. In Fig. 3, the elastic part of the deformation represents approximately 0.4% of the total deformation at ultimate capacity and 4.5% of the deformation at $0.4 \times M_R$, with the elastic threshold defined as in Abadie (2015). Hence, the plastic deformation is the principal focus for the modelling approach described here.

Loading rate effect

The response of soil to shearing can possibly involve rate-dependency effects, which are usually incorporated in soil structure interaction models using viscosity (e.g. Hardin, 1965). This effect is usually discarded in pile design, with very few data available in the published literature addressing the phenomenon. Rate dependency, manifested as a creep response at constant load during the incremental tests, was explored by comparison of the response of the continuous and incremental tests shown in Fig. 5. The incremental tests results (MCr1-3), which cover a range of loading periods, are represented by the final displacement at each load step for clarity, with further information on the creep periods available in Abadie (2015). The incremental responses show close agreement with the continuous test data (MCo). Any disparity between the curves appears within experimental error (less than 10%), showing that tests with the creep phases do mimic a continuous load of 0.1 Hz.

For this pile geometry and load frequency, it therefore appears that rate-dependency is relatively small in dry sand (as opposed to saturated sand where partial drainage may result in a stronger influence of strain rate). Hence, it is expected that the energy dissipation of the soil-pile interaction is rate-independent and of a hysteretic nature, as is common for soils (e.g. Kokusho, 1980, Tatsuoka et al., 1978, Ishihara, 1996). Rate-dependency also becomes apparent within the cyclic loading response by the rounding of the load peaks of a continuous load-displacement curve (e.g. Hassan and Kyriakides, 1992). However, as shown later in Fig. 12a, this effect is very limited in the tests reported here.

Short-term hysteretic behaviour

Plastic behaviour

The plastic behaviour of non-degrading materials is commonly modelled in plasticity theory using principles of kinematic and isotropic hardening (separately or combined). Either hardening mechanism can be used to model a monotonic loading curve, and to distinguish between them experimentally it is necessary to explore unloading and reloading behaviour. It is expedient to explore kinematic hardening first, as simple rules and testing procedures may quickly establish whether this mechanism predicts the response adequately. Additionally, soil behaviour has been modelled

extensively using kinematic hardening based approaches (e.g. Prevost, 1977, Pyke, 1979, Vucetic, 1990), using techniques such as the multi-surface nested models (Mróz, 1967, Iwan, 1967).
Masing (1926) established that models that employ pure kinematic hardening automatically give rise to the following rules: (i) the unloading and reloading curves are defined based on the initial loading curve, called the *backbone curve*, enlarged by a factor of 2; (ii) after any load reversal, the tangent shear modulus is the same as the initial shear modulus of the backbone curve. Therefore, perfectly symmetric loading test results generally provide a good estimation of whether kinematic hardening models provide a good prediction of the results, simply by comparing the initial curve (factored by 2) with the unloading-reloading curves.
Test H0 aims to identify whether the above framework applies to the laboratory pile response at high loading magnitude. The results are displayed in Fig. 6, with the dashed line resulting from the reversed loading data (the unloading path), scaled down by a factor of two and plotted from the origin. The graph shows the scaled unloading curve gives a close approximation of the original loading with the response conforming closely to the Masing rules. It is difficult to assess whether the slight differences observed can be interpreted using another mechanism (such as isotropic hardening or ratcheting) or ascribed to experimental error. Clearly, however, a good first approximation of the pile response to symmetric cyclic loading can be obtained using kinematic hardening.
The two Masing rules formulated above describe the response to regular cyclic loading of constant amplitude only. For general loading, Pyke (1979) contributed to the above framework with two additional statements: (iii) when exceeding the maximum past load, the unloading or reloading curve follows that of the backbone curve until the next load reversal; (iv) each time an unloading or reloading path intersects a curve from a previous cycle, the stress-stain curve then follows that curve. Rules (i)-(iv) are referred to as *extended Masing rules* and imply that symmetric cyclic stress-strain behaviour can be entirely defined provided the backbone curve is chosen properly. It is important to note that the extended Masing rules arise naturally from kinematic hardening and need not be introduced as separate assumptions. To investigate whether the pile-soil response conforms to these extended rules, a 2-way cyclic test at increasing load magnitude was performed (Test HIM) and the results are displayed in Fig. 7 and superimposed with the results of test H0. The graph shows that, on passing extreme load levels from previous cycles, the reloading path follows that of the backbone curve (test H0) and therefore, the pile response complies with the extended Masing rules. It is also clear that the secant stiffness k_0 reduces with load increase, due to the shape of the backbone curve. Similar conclusions are obtained during non-symmetric cyclic loading tests at increasing magnitudes. This is shown in Fig. 8 (test H1IM), where it is observed that (a) the tangent modulus of each reloading curve is equal to the initial modulus E_0 and (b) the reloading paths follow the backbone curve when exceeding the maximum past load. In addition, compared to the symmetric loading test, cycling at non-zero mean load leads to accumulated deformation: the hysteresis loops do not close and the maxima of each cycle are not super-imposed. This phenomenon, called ratcheting, cannot be captured solely by kinematic hardening, and needs to be more thoroughly characterised before it can be included robustly within any theoretical modelling framework.

Hysteretic damping

Hysteretic damping of soils is commonly studied through the damping ratio (e.g. Ishihara, 1996), which can be derived from Figs. 6, 7 and 8 for pile foundations loaded at high magnitude and at a frequency of 0.106 Hz. The damping ratio is a dimensionless parameter commonly used to measure how vibrations decay due to energy dissipation. It is defined as the ratio between the dissipated energy during a cycle (the area enclosed by the hysteresis loop, A_{hys}) over the "stored elastic energy" (hashed area on Fig. 6, A_{el}) (e.g. Vucetic and Dobry, 1991, Ishihara, 1996):

$$D_a = \frac{1}{4\pi}\frac{A_{hys}}{A_{el}} = \frac{A_{hys}}{2\pi k_0 \theta_{\max}^2} \tag{13}$$

For test H0, this gives D_{a0}=0.28 and Fig. 10 shows that, for cyclic load magnitudes above 30% of static capacity, the damping ratio appears to be almost independent of the load magnitude (test HIM).

Accepted manuscript doi:
10.1680/jgeot.16.p.325

For test H1IM, the above definition was adapted for non-symmetric cyclic loading according to Fig. 9. The results for test H1IM validate the definition of damping ratio adopted for non-symmetric cyclic loads, and show limited effect of load magnitude. In Fig. 10, the average value is damping ratio 0.3. This result compares well with similar small-scale laboratory tests performed on suction caissons in dense sand where comparable hysteresis loop shape evolutions and a damping ratio of 0.2 were observed (Byrne 2000, Chapter 5).

In Fig. 7, the corresponding pile displacement at peak load ranges from 0.3% to 3.5% of the pile diameter. Assuming this reflects the order of the shear strain magnitude within the ground, this fairly high shear strain amplitude for which the damping ratio of sand measured with torsional shear test and/or resonant column apparatus is typically around 0.25 (Hardin and P. Drnevich, 1972, Kokusho, 1980, Vucetic and Dobry, 1991), with higher values expected at low confining pressure (Tatsuoka et al., 1978) and limited effect of the relative density (e.g. Ishihara, 1996). In the specific case of Leighton Buzzard sand, the maximum damping ratio value reported in the literature is 0.2 and was obtained for a dry sand of particle size close to that used in the reported experiments, at a shear strain of 0.05% and confining pressure of 150kPa (Cavallaro et al., 2001). This compares reasonably well with the damping ratio observed in Fig. 10 for the global soil-pile interaction.

Also, it is expected that the hysteresis loop shape for piles in the field might be controlled by other mechanisms not captured in the laboratory, such as gapping. Large-scale field tests would enable the laboratory model scale pile behaviour to be related to that of real offshore wind monopiles in a similar manner to the work of Kelly et al. (2006) for suction caissons.

Long-term continuous cyclic loading

Pile response

The pile response to cyclic loading is described in terms of (a) deformation (b) secant stiffness and (c) hysteresis loop area as defined on Fig. 11. A typical moment-rotation curve (test CMLT3) is displayed in Fig. 12a, showing that the hysteresis loop shape develops with cycle number while the pile rotation increases. The initial loading-unloading cycle is referenced as 0 and refers to the initial monotonic loading and hysteresis behaviour. Pile deformation due to cyclic loading only is best estimated using the accumulated rotation $\Delta\theta=\theta_N-\theta_0$. The evolution of $\Delta\theta$ observed for the three long-term cyclic tests (CMLT1-3, N~100,000 cycles) is displayed in Fig. 12b. As previously observed (e.g. LeBlanc et al., 2010b, Cuéllar, 2011, Klinkvort, 2012, Peralta, 2010) the accumulated deformation of the pile increases with cycle number. The data have been fitted using the empirical power-law proposed by LeBlanc et al. (2010b) ($\Delta\tilde{\theta} = \tilde{T}_{bc} N^{0.31}$) with the predicted results displayed by dotted lines. This shows good agreement to the experimental data for the first 10,000 cycles. However, beyond this limit, the experimental data depart from the predictions and the accumulated rotation due to each cycle is less significant.

It is useful to quantify this decrease and estimate whether the pile still accumulates deformation after large cycle numbers or reaches an asymptotic value. This is important for constitutive model development, as constant accumulation of permanent strain with cycle number, or ratcheting, is difficult to model, while stabilisation after a given number of cycles, either accommodation or adaptation, can be captured using combined isotropic and kinematic hardening. The evolution of the rate of increase of accumulation, $\delta\tilde{\theta} = \tilde{\theta}_{N+1} - \tilde{\theta}_N$, is shown in Fig. 12c for tests CMLT1-3. The graph shows that the rate continues to decrease with cycle number. However, for the load cases studied here and the number of cycles involved, the rate never decays to zero as N increases. This demonstrates that the pile experiences ratcheting with cyclic loading at non-zero mean load, at least for the first 100,000 cycles. This compares favourably with other findings, in particular the test results from (Cuéllar, 2011), where more than 1,000,000 cycles were performed on a model test pile. These test results were re-processed by Abadie et al. (2015) in terms of rate of increase and demonstrate that the above conclusion extends to very large cycle number.

Accepted manuscript doi:
10.1680/jgeot.16.p.325

Fig. 12d displays the evolution of the secant stiffness with cycle number, showing two trends: a sharp increase during the first 50 cycles, then a change of slope, leading to a steady-state and slow increase over the rest of the test. The second phase of response matches with the logarithmic law proposed by LeBlanc et al. (2010b). The testing equipment used by LeBlanc et al. (2010a,b), which used dial gauge measurements rather than continuously recorded LVDT measurements, perhaps did not enable sufficiently accurate capture of the initial cycles of loading. Klinkvort (2012) also observed a logarithmic increase of the secant stiffness with cycle number, however, the reported data points are too sparse within the 0 to 50 cycles region to correlate with the findings reported here. However, the two phases identified in Fig. 12d demonstrate a change in the foundation behaviour, with significant stiffening occurring during the first few cycles. Note that these results may be specific to the low density of the sand samples employed, and need to be investigated further for other soil conditions.
In addition to the secant stiffness, the hysteresis loop shape evolution can be described in terms of loop area. This parameter provides important information for fatigue design as it is directly proportional to the damping ratio of the foundation. The results are presented in the normalised form according to:

$$\tilde{A} = \frac{A}{L^3 D\gamma'}\sqrt{\frac{p_a}{L\gamma'}} \tag{13}$$

The data for tests CMLT1-3 are displayed in Fig. 12e and show a tightening of the loop shape with cycle number, following a pattern of exponential decay. The data fitting, shown with the dotted lines, correspond to:

$$\tilde{A} = \tilde{A}_r \, N^{-0.15} \tag{13}$$

where $\tilde{A}_r$ is a dimensionless function. The data were re-processed in terms of damping ratio according to the definition of Fig. 9, and the results (Fig. 12f) indicate that the net amount of dissipated energy decreases with cycle number, in a similar fashion as the hysteresis loop area. The fitted curves correspond to the same relationship as Equation (13), with the same exponent value. It is also noted here that the graph shows limited effect of the load magnitude on the damping ratio evolution, similarly to Fig. 10.
As both the secant stiffness and the loop area contribute to the description of the hysteresis loop shape, it is interesting to investigate whether these two parameters are linked to one another. Fig. 13 shows that, as a first approximation, the evolution of the loop area can be considered as a linear function of the secant flexibility $1/\tilde{k}$ minus the initial flexibility $1/\tilde{E}_0$. This is justified more rigorously through constitutive modelling equations in Abadie (2015). This result implies that, when modelling the evolution of the hysteresis loop shape with cyclic loading, the stiffening of the response and tightening of the hysteresis loop must be treated as linked phenomena.
Finally, Fig. 12b-c demonstrate that load magnitude has a significant impact on the amount of accumulated deformation caused by cyclic loading. This was investigated further by LeBlanc et al. (2010b) and needs to be accounted for in modelling methods.

Accepted manuscript doi:
10.1680/jgeot.16.p.325

Effect of cyclic loading on monotonic response

The impact of continuous cyclic loading (ratcheting and evolution of the hysteresis loop shape) on the subsequent monotonic response of the pile is an important area to explore. Continuous cyclic tests, followed by a monotonic load, investigated both the effect of cycle number (CMC1-5, CMLT2) and load magnitude (CMLT1-3). The results are displayed in Fig. 14a and b respectively. Only the reloading monotonic curves are plotted and the past cyclic load history is indicated by a dashed horizontal line, with ordinate of the cyclic load magnitude, and the abscissa of each reloading curve, plotted from the final cyclic rotation at minimum peak load. Fig. 14a shows that, on reloading and exceeding the maximum cyclic load, the monotonic curves all approximately rejoin the backbone curve, and the tangent shear modulus is the same as the initial modulus, despite the changes caused by non-symmetric cyclic loading. The graph illustrates a very sharp increase in secant stiffness during the first cycle and then a second softer change between cycle 10 and 100, after which the yield load appears to remain unchanged and equal to the maximum cyclic load. This is consistent with the findings from Fig. 12d.

Finally, the plot shows that the accumulation of ratcheting deformation takes the reloading curve away from the backbone curve while the stiffening phenomenon actually brings it closer. Hence, a change in cyclic load magnitude does not appear to alter the Masing behaviour significantly (Fig. 14b), however, it might generate such substantial deformation, that the reloading curve never re-joins the backbone curve within the relevant loading range (case of test CMLT3, Fig. 14b).

The above results demonstrate that determination of the monotonic response following cyclic loading results from a competition between (i) Masing behaviour, (ii) ratcheting and (iii) progressive stiffening of the response. This result is of great importance as it strongly calls into question current practice where pile capacity is often degraded with cycle number (e.g. degrading cyclic factor A=0.9 recommended in DNV, 2016), and actually shows very limited degradation of pile capacity following cyclic loading.

Multi-amplitude cyclic loading

Effect of load history

The extension of the above work is to explore how the framework applies to variable amplitude load series. The first three tests studied here (MALL1-3) involve three series of load cycles (Table 5) and investigate the effect of load history by exploring the order in which they are applied. First, Fig. 15a displays the normalised rotation of the three tests. This graph shows that the load history has a modest effect, with slightly different final displacements for each test, in the order MALL2>MALL3>MALL1. Fig. 15b-c shows the evolutions of the secant stiffness and hysteresis loop area for the three tests and interestingly, the curves super-impose for the same load magnitude and cycle number. This suggests that, for the load sequences investigated, the hysteresis loop shape is not affected by the load history, and solely depends on the load magnitude and cycle number.

Finally, Fig. 15d-f display the moment-rotation curves of the three tests compared with the monotonic backbone curve. The figures clearly show that the response compares favourably to the results previously described, and mostly, that on reloading and exceeding the previous maximum load, the response re-joins that of the backbone curve. This is an important feature of the pile response which, despite ratcheting, conforms to the extended Masing behaviour. Besides, the order of tests based on final displacement observed in Fig. 15a can now be interpreted. In general, the largest load is responsible for the largest contribution to the pile deformation. This is due to the shape of the backbone curve, with a softer response towards higher load. However, the *larger* the load history before the extreme event, the stiffer the subsequent response to the extreme load event, and therefore, the lower the induced deformation. The test where the extreme event occurs last is the one that induces the least displacement, and accordingly, the test where the largest load appears first produces the largest pile rotation. It remains to define what the term "larger" highlighted in italics means, *i.e.* whether it is in terms of cycle number, load magnitude or both, and also, whether there are thresholds after which the response remains unchanged.

The tests MALL1, 2, 4, 5 and 6 explore these ideas further by examining the influence of an initial large load packet at different cycle number (MALL1,2 4 and 5) and load magnitude (MALL1, 4 and 6) on a 100C series (Table 5). Fig. 16a displays the rotation of the 100C load series, plotted from the origin (previous load history discarded), for tests involving an initial series of E cyclic load at a range of cycle number. The graph illustrates the intuitive conclusion that the number of previous load cycles reduces the ratcheting induced by the subsequent cyclic load, with a significant change in response dependent on applying 10 cycles of E or 100 cycles of E. This relates to the change in stiffness observed in Fig. 12d and Fig. 14a-b, implying that the progressive stiffening of the response competes with ratcheting, retarding the accumulation of pile deformation. The results correlate favourably with conclusions regarding the order of pile final displacement between tests MALL1-3.
Finally, tests MALL1, 4 and 6 investigate the influence of previous load magnitude on the 100C load series response for the same number of cycles. Compared to Fig. 16a, the test results on Fig. 16b demonstrate that the ratcheting rate is not greatly affected by larger previous load magnitude for the sequence investigated. This indicates that the primary mechanism reducing the ratcheting rate, and which should be accounted for in design, is the effect of cycle number and magnitude.

Alternating operational and storm load series

The above conclusions were extended to load cases involving alternating long-term FLS, short-term SLS and single ALS load events through tests MASL1-3. The evolutions of the total pile deformation (Fig. 17a) are represented for each test with light grey lines, while the darker lines represent the maximum displacement of each test. The figure shows that the final displacement of the three tests is close. This means that the lowest magnitude load history does not affect the pile response much and that the final deformation is mostly due to the largest magnitude load series (1E and 100C). Similar conclusions were reached by Leblanc et al. (2010a). This is further verified on Fig 17b-d, where the effect of small load amplitude is virtually negligible and the response reaches an accommodated cyclic loop. This phenomenon can be explained by the stiffening of the response induced by the large load cycles, which reduces the deformation induced by the subsequent cycles at small magnitude, such as previously observed in Fig. 14 and 15.
In conclusion, Fig. 17b-d display similar trends to those previously observed, featuring a competition between (a) Masing rule, (b) ratcheting and (c) progressive stiffening of the response. This implies that, if a constitutive model is able to capture accurately the response to continuous cyclic loading, prediction to multi-amplitude load cases using this model should then be straightforward.

Accepted manuscript doi:
10.1680/jgeot.16.p.325

Conclusions

The experimental work presented in this paper demonstrated that the response of large diameter monopiles in drained sand, subjected to continuous cyclic lateral loading, is dominated by:

(a) Masing behaviour when subjected to symmetric cyclic loading. Some features of the extended Masing rules endure after large number of non-symmetric cyclic loading scenarios, and in particular: (a) re-joining of the backbone curve when exceeding the maximum historic cyclic load and (b) no change to the initial tangent stiffness.
(b) Increase in accumulated ratcheting deformation due to cyclic loading at non-zero mean applied load, with the rate of ratcheting decreasing with cycle number but not decaying to zero, and depending on the cyclic load magnitude
(c) Change in hysteresis loop shape, including an increase in secant stiffness and reduction of the hysteresis loop area, mostly during the first 50 cycles of a given load magnitude

The above points appear to be the key mechanisms driving the pile response under cyclic loading and need to be accounted for in any detailed modelling approach. They occur all at once and compete with each other, leading the pile response to depart or not from the initial backbone curve. In addition, for the pile geometry and sample conditions tested, it was shown that the response is insensitive to loading rate effects. The pile response to a series of cyclic loads of varying magnitude is a direct result from Masing behaviour and ratcheting behaviour. This means that if the first two phenomenon are accurately captured in modelling, the behaviour of the pile under multi-amplitude cyclic loading would follow with no additional effort.

The paper outlines experimental methods that can be used for identifying key mechanisms for the development of appropriate constitutive models. Such models, applied to as a macro-element for monopile response, are explored in detail in Abadie (2015) and Houlsby et al. (2017). The work described here was completed at model scale to explore phenomenological behaviour. Future work on large-scale model piles in the field would be extremely useful to confirm this framework translates to larger scale and to provide correlations with numerical values at full scale. Finally, this paper addresses cyclic loading from the point of view of the macro-pile behaviour. It would be of great interest to analyse the soil behaviour down the pile and correlate the macro-response observed in this paper to the local pile behaviour, and also to soil element behaviour. This approach would be beneficial for model calibration purposes, but its development is still in progress (see e.g. Nikitas *et al.* 2017); it can be informed by a prior understanding of the macro-behaviour of the pile, as described in this paper.

Implications for design

The work presented in this paper provides insight into rigid pile response that has direct implications for current design methodologies for the prediction of pile response to (cyclic) lateral loading:

(i) The pile response exhibits a hysteretic response that corresponds to energy loss when the pile deforms the soil. So far, this is not accounted for by the *p-y* method (DNV, 2016) but needs to be addressed to estimate more accurately the soil damping.
(ii) The initial modulus of the foundation appears to be unaltered by cyclic loading and can therefore be used in design for cyclic loads where relevant.
(iii) Design for ultimate capacity, after series of small repeated loads, does not require the use of degradation factors, as the monotonic capacity at large displacements appears to be unchanged.
(iv) A short series of large loads reduces significantly the accumulated deformation caused by subsequent cyclic loads at lower magnitude.
(v) Repeated cyclic loads at small magnitude reduce the impact of extreme load events on the pile deformation. This could signify that the time between installation of the foundation and the rest of the turbine could be beneficial for the lifetime of the turbine.

Acknowledgements

The first author is grateful for the generous funding and support for DPhil studies from EDF R&D and EDF Energies Nouvelles

Accepted manuscript doi:
10.1680/jgeot.16.p.325

List of notation

A, A_{hys}	FL.rad	Hysteresis loop area
A_{el}	FL.rad	Area corresponding to elastic energy stored in system
D	L	Pile diameter
D_a	-	Damping ratio
E_0	FL.rad^{-1}	Initial tangent shear modulus
E_pI_p	FL^2	Bending Stiffness
E_S	FL^{-2}	Soil modulus at level of pile tip
G_0	FL^{-2}	Shear modulus at small strain
h_e	L	Load eccentricity
k	FL.rad^{-1}	Secant stiffness
K_R	-	Pile relative stiffness
L	L	Pile embedded length
M	FL	Moment load at mud-line
M_{max}, M_{min}	FL	Maximum and minimum cyclic moment at mud-line
M_R	FL	Static moment capacity
N	-	Number of cycles
p_a	FL^{-2}	Atmospheric pressure
γ'	FL^3	Effective unit weight
ζ_b	-	Maximum load magnitude during cyclic loading $\zeta_b=M_{max}/M_R$
ζ_c	-	Cyclic load amplitude $\zeta_c=M_{min}/M_{max}$
θ	rad.	Pile rotation
θ_{max}	rad.	Pile rotation at maximum cyclic load
$\tilde{X}$	Normalised parameter X	

References

Abadie, C. N. (2015) Cyclic Lateral Loading of Monopile Foundations in Cohesionless Soils. DPhil Thesis, University of Oxford.

Abadie, C. N., Byrne, B. W. & Levy-Paing, S. (2015) Model pile response to multi-amplitude cyclic lateral loading in cohesionless soils. 3rd Int. Symp. on Frontiers in Offshore Geotechnics (ISFOG), Oslo, Norway, pp. 681-686.

API (2010) Recommended Practice for Planning, Designing and Constructing Fixed Offshore Platforms, RP2A-WSD, Washington.

Bolton, M. D. (1986) Strength and dilatancy of sands. Géotechnique 36(1):65-78.

Burd, H. J., Byrne, B. W., Mcadam, R. A., Houlsby, G. T., Martin, C. M., Beuckelaers, W. J. a. P., Zdravkovic, L., Taborda, D. M. G., Potts, D. M., Jardine, R. J., Gavin, K., Doherty, P., Igoe, D., Skov Gretlund, J., Pacheco Andrade, M. & Muir Wood, A. (2017) Design aspects for monopile foundations In Proceedings of TC209 Workshop - Foundation Design of Offshore Wind Structures.

Byrne, B. W. (2000) Investigations of Suction Caissons in Dense Sand. DPhil Thesis, University of Oxford.

Byrne, B. W. & Houlsby, G. T. (2004) Experimental investigations of the response of suction caissons to transient combined loading. J. of Geotechnical and Geoenvironmental Engineering 130(3):240-253.

Byrne, B. W., Mcadam, R., Burd, H. J., Houlsby, G. T., Martin, C. M., Gavin, K., Doherty, P., Igoe, D., Zdravković, L., Taborda, D. M. G., Potts, D. M., Jardine, R. J., Sideri, M., Schroeder, F. C., Muir Wood, A., Kallehave, D. & Skov Gretlund, J. (2015) Field testing of large diameter piles under lateral loading for offshore wind applications. In Proceedings of the Fifteenth European Conference on Soil Mechanics and Geotechnical Engineering (ECSMGE), Edinburgh, UK.

Cavallaro, A., M, M. & R, M. (2001) Static and Dynamic Properties of Leighton Buzzard Sand from Laboratory Tests.

Cook, M. F. & Vandiver, J. K. (1982) Measured and Predicted Dynamic Response of a Single Pile Platform to Random Wave Excitation In Proceedings of Proceedings of the 14th annual offshore technology conference, pp. 637-643.

Cuéllar, P. (2011) Pile Foundations for Offshore Wind Turbines: Numerical and Experimental Investigations on the Behaviour under Short-Term and Long-Term Cyclic Loading. In Federal Institute for Materials Research and Testing, Berlin.

Dietrich, T. (1982) Incremental parabolic hardening of psammic material; Application to laterally loaded piles in sand. In IUATAM Conference on Deformation and Failure of Granular Materials.), Delft, pp. 13-22.

DNV (2016) Offshore Standard DNVGL-ST-0126, Support structures for wind turbines (current edition, April 2016).

EWEA (2009) The Economics of Wind Energy. pp. 156.

Germanischer Lloyd (2005) Overall Damping for Piled Offshore Support Structures.

Hardin, B. (1965) The nature of damping in sands. Soil Mechanics and Foundations 91(1):63-98.

Hardin, B. & P. Drnevich, V. (1972) Shear modulus and damping in soil: Measurement and parameter effects. Soil Mechanics and Foundations 98(6):603-624.

Hassan, T. & Kyriakides, S. (1992) Ratcheting in cyclic plasticity, part I: Uniaxial behavior. International Journal of Plasticity 8(1):91-116.

Houlsby, G. T., Abadie, C. N., Beuckelaers, W. J. a. P. & Byrne, B. W. (2017) A model for nonlinear hysteretic and ratcheting behaviour. International Journal of Solids and Structures 120(Supplement C):67-80.

Ishihara, K. (1996) Soil behaviour in earthquake geotechnics. Clarendon Press.

Iwan, D. W. (1967) On a class of models for the yielding behaviour of continuous and composite systems. Journal of Applied Mechanics, ASME 34:612-617.

Kelly, R. B., Houlsby, G. T. & Byrne, B. W. (2006) A comparison of field and laboratory tests of caisson foundations in sand and clay. Géotechnique 56(9):617-626

Klinkvort, R. T. (2012) Centrifuge modelling of drained lateral pile-soil response. DTU.

Kokusho, T. (1980) Cyclic triaxial test of dynamic soil properties for wide strain range SOILS AND FOUNDATIONS 20(2):45-60.

Leblanc, C., Byrne, B. W. & Houlsby, G. T. (2010a) Response of Stiff Piles to Random Two-Way Lateral Loading. Géotechnique 60(9):715-721.

Leblanc, C., Houlsby, G. T. & Byrne, B. W. (2010b) Response of Stiff Piles in Sand to Long-term Cyclic Lateral Loading. Géotechnique 60(2):79-90

Masing, G. (1926) Eiganspannungen und Verfestigung beim Messing. In Proceedings for the 2nd International Congress of Applied Mechanics.

Mróz, Z. (1967) On the description of anisotropic workhardening. Journal of the Mechanics and Physics of Solids 15(3):163-175.

Nikitas, G., Arany, L., Aingaran, S., Vimalan, J. & Bhattacharya, S. (2017) Predicting long term performance of offshore wind turbines using cyclic simple shear apparatus. Soil Dynamics and Earthquake Engineering 92:678-683.

Peralta, P. (2010) Investigations on the Behavior of Large Diameter Piles under Long-Term Lateral Cyclic Loading in Cohesionless Soil. University of Hannover.

Poulos, H. G. (1982) Single pile response to cyclic lateral load. J. of Geotechnical and Geoenvironmental Engineering 108:355-375.

Prevost, J.-H. (1977) Mathematical modelling of monotonic and cyclic undrained clay behavior. International Journal for Numerical and Analytical Methods in Geomechanics 1(2):195-216.

Pyke, R. M. (1979) Nonlinear soil models for irregular cyclic loadings. J. Geotechnical Engineering Division, ASCE 105(GT6, Proc Paper, 14642):715-726.

Rovere, M. (2004) Cyclic loading test machine for caisson suction foundations. Centrale Lille and Politechnico di Milano.

Schnaid, F. (1990) A study of the cone-pressuremeter test in sand.) University of Oxford.

Tarp-Johansen, N. J., Andersen, L., Christensen, E. D., Mørch, C., Kallesøe, B. & Frandsen, S. (2009) Comparing sources of damping of cross-wind motion. Proceedings European Offshore Wind Conf., Stockholm, Sweden.

Tatsuoka, F., Iwasaki, T. & Takagi, Y. (1978) Hysteretic damping of sands under cyclic loading and its relation to shear modulus. Soils and Foundations 18(2):25-40.

Vucetic, M. (1990) Normalized behavior of clay under irregular cyclic loading. Canadian Geotechnical Journal 27(1):29-46.

Vucetic, M. & Dobry, R. (1991) Effect of soil plasticity on cyclic response. J. of Geotechnical Engineering 117(1):89-107.

Accepted manuscript doi:
10.1680/jgeot.16.p.325

List of Tables

Table 1. Parameter normalisation for scaling of 1-g model tests (from LeBlanc et al., 2010b)

Parameter	**Normalised form**
Moment Loading	$\tilde{M} = \frac{M}{L^3 D\gamma'}$
Rotation [rad.]	$\tilde{\theta} = \theta\sqrt{\frac{p_a}{L\gamma'}}$
Displacement	$\tilde{\upsilon} = \frac{\upsilon}{D}\sqrt{\frac{p_a}{L\gamma'}}$
Secant stiffness	$\tilde{k} = \frac{k}{L^{5/2} D\sqrt{p_a\gamma'}}$
Eccentricity	$\tilde{h}_e = \frac{h_e}{L}$

Table 2. Properties of Yellow D14/25 Leigthon Buzzard (Schnaid, 1990)

Property	**Values**
Minimum dry unit weight γ_{min} (kN/m^3)	14.65
Maximum dry unit weight γ_{max} (kN/m^3)	17.58
Specific Gravity G_S	2.65
Critical angle of friction ϕ_{cr} (°)	34.3
Mean particle size d_{50} (mm)	0.80
Coefficient of uniformity C_u	1.35

Accepted manuscript doi:
10.1680/jgeot.16.p.325

Table 3. Model piles properties

Property	Values
Embedded length L (m)	0.36
Load eccentricity h_e (m)	0.43
Pile diameter D (mm)	77
Wall thickness t (mm)	2
Young's Modulus E_p (MPa)	120

Table 4. Test Programme

Test No.	Test method	Loading description		
Phase 1 – Monotonic tests				
MCr1	Incremental (15min)	M_{max} = 30 Nm		
MCr2	Incremental (3min)	M_{max} = 30 Nm		
MCr3	Incremental (1min)	M_{max} = 27 Nm		
MCo	Continuous	M_{max} = 29 Nm		
MCo1	Continuous	M_{max} = 29.4 Nm		
MCo2	Continuous	M_{max} = 28.5 Nm		
MCo3	Continuous	M_{max} = 29 Nm		
Phase 2 – Hysteresis behaviour				
H0	Incremental (3/1min)	Symmetric reversed loading 1 cycle, (M_{max} = 23.1 Nm)		
HIM	Incremental (3/1min)	Symmetric reversed loading increasing magnitudes 4 cycles, ($M_{max,cycle}$ = 10.7 Nm, 14.8 Nm, 19.1 Nm, 23.2		
H1IM	Continuous	1-way loading, increasing magnitudes, 7 cycles ($M_{max,cycle}$ = 8.2 Nm, 11.3 Nm, 12.9 Nm, 16.7 Nm, 19.8 Nm, 23.2Nm, 28.8 Nm)		
Phase 3 – Continuous cyclic		ζ_h	ζ_c	N
CMC1	Continuous+Monotonic	0.42	0.18	1
CMC2	Continuous+Monotonic	0.42	0.18	10
CMC3	Continuous+Monotonic	0.42	0.18	100
CMC4	Continuous+Monotonic	0.42	0.18	1000
CMC5	Continuous+Monotonic	0.42	0.18	10000
CMLT1	Continuous+Monotonic	0.31	0.24	100, 000
CMLT2	Continuous+Monotonic	0.42	0.18	100, 000
CMLT3	Continuous+Monotonic	0.47	0.13	100, 000
Phase 4 – Multi-amplitude cyclic tests				
Series of large load events				
MALL1	Continuous	100 × C − 10 × D − 1 × E		

MALL2	Continuous	$1 \times E - 100 \times C - 10 \times D$
MALL3	Continuous	$10 \times D - 1 \times E - 100 \times C$
MALL4	Continuous	$10 \times E - 100 \times C$
MALL5	Continuous	$100 \times E - 100 \times C$
MALL6	Continuous	$10 \times F - 100 \times C$
Combination of long-term small and short-term large load events		
MASL1	Continuous	$1000 \times A - 100 \times C - 1 \times E$
MASL2	Continuous	$100 \times C - 1 \times E - 1000 \times A$
MASL3	Continuous	$1 \times E - 100 \times C - 1000 \times A$

Table 5. Load cases for multi-amplitude cyclic tests

Load case	ζ_b	ζ_c	**Test Nos.**
A	0.3	0.11	MASL1,2,3,6
B	0.38	0.08	MASL4
C	0.48	0.00	MALL1-6; MASL1-5
D	0.59	0.03	MALL1,2,3
E	0.69	0.00	MALL1-5; MASL1-5
F	0.83	0.00	MALL6

Accepted manuscript doi:
10.1680/jgeot.16.p.325

Table 6. Relevant properties of the monotonic tests selected from LeBlanc et al. (2010b), Klinkvort (2012), Peralta (2010) and Burd et al. (2017)

Test No.	L (m)	D (m)	L/D	h_e (m)	γ' (kNm^2)	D_R (%)
LeBlanc et al. (2010b)						
1	0.36	0.08	4.5	0.035	14.7	4
2	0.36	0.08	4.5	0.15	14.7	4
3	0.36	0.08	4.5	0.28	14.7	4
4	0.36	0.08	4.5	0.43	14.7	4
5	0.36	0.08	4.5	1.2	14.7	4
15	0.36	0.08	4.5	0.43	15.6	38
Klinkvort (2012)						
22	0.132	0.022	6	0.33	16.4	90
23	0.168	0.028	6	0.42	16.6	90
24	0.204	0.034	6	0.51	16.6	90
25	0.240	0.040	6	0.6	16.4	84
Peralta (2010)						
1	0.2	0.06	3.33	0.24	14.74	40
2	0.2	0.06	3.33	0.24	15.34	60
3	0.4	0.06	6.67	0.24	14.74	40
4	0.4	0.06	6.67	0.24	15.34	60
5	0.5	0.06	8.33	0.24	14.74	40
6	0.5	0.06	8.33	0.24	15.34	60
PISA, Dunkirk Sand (Burd et al., 2017)						
DM4	4.0	0.76	3.0	10	NA	75

Accepted manuscript doi:
10.1680/jgeot.16.p.325

List of Figures

Figure 14. Influence of (a) cycle number and (b) cyclic load magnitude on monotonic response

Figure 15. MALL 1-3 Multi-amplitude cyclic test results: Evolutions of the (a) total pile rotation, (b) secant stiffness and (c) hysteresis loop area. Moment-rotation curves for test (d) MALL1, (e) MALL2 and (f) MALL3

Figure 16. Comparison of the rotation evolution during the 100C series for (a) four multi-amplitude tests involving different loading histories and (b) three multi-amplitude tests involving different loading magnitude histories

Figure 17. MASL 1-3 Multi-amplitude cyclic test results: (a) Evolutions of the total pile rotation. Moment-rotation curves for test (b) MASL1, (c) MASL2 and (d) MASL3

Accepted manuscript doi:
10.1680/jgeot.16.p.325

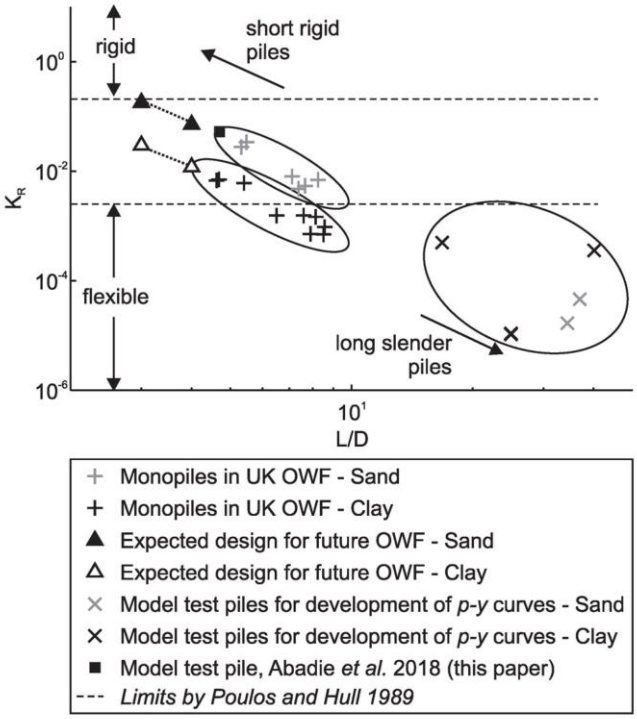

Fig1

Accepted manuscript doi:
10.1680/jgeot.16.p.325

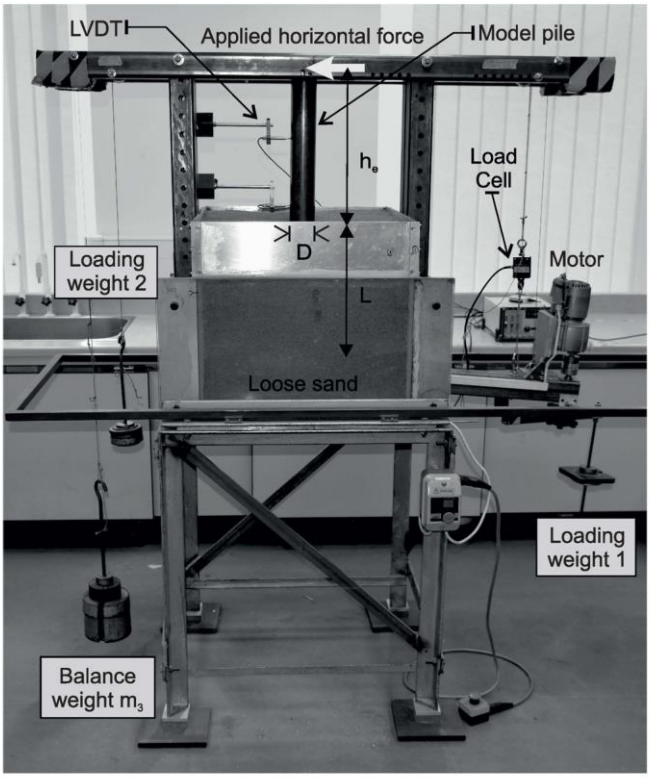

Fig2

Accepted manuscript doi:
10.1680/jgeot.16.p.325

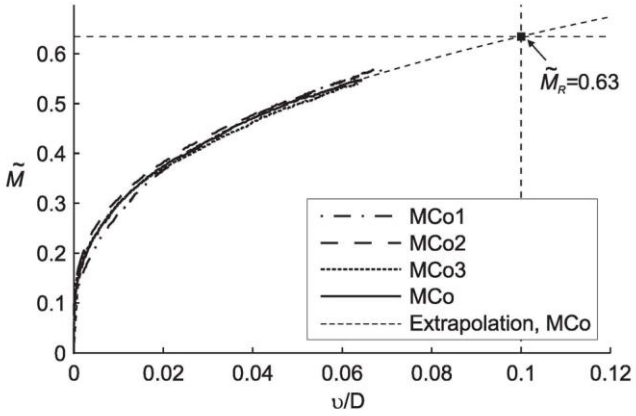

Fig3

Accepted manuscript doi:
10.1680/jgeot.16.p.325

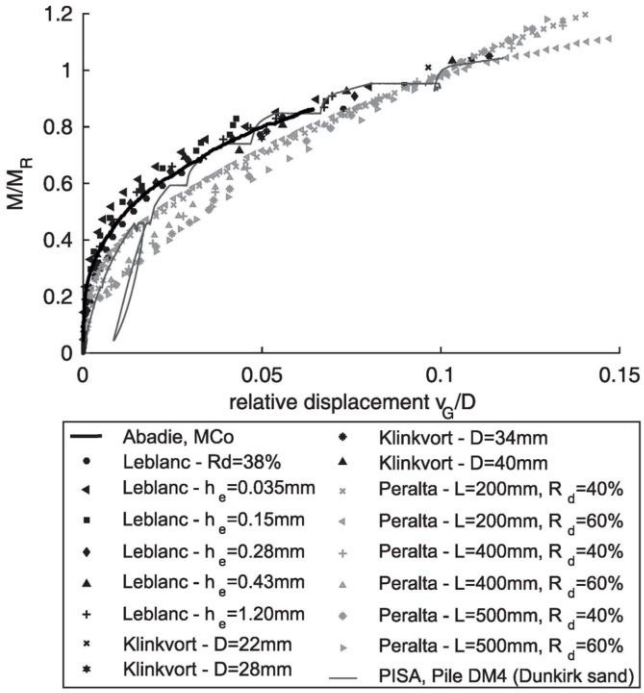

Fig4

Accepted manuscript doi:
10.1680/jgeot.16.p.325

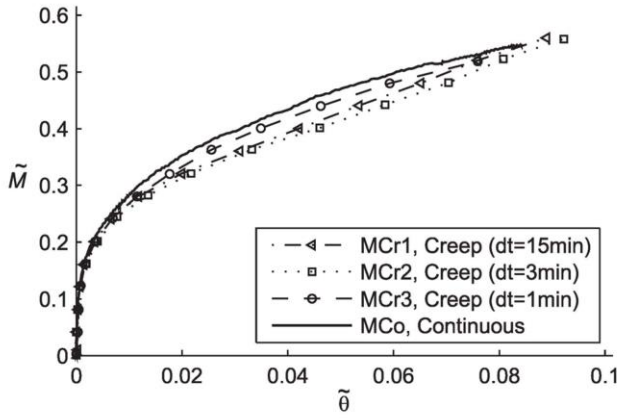

Fig5

Accepted manuscript doi:
10.1680/jgeot.16.p.325

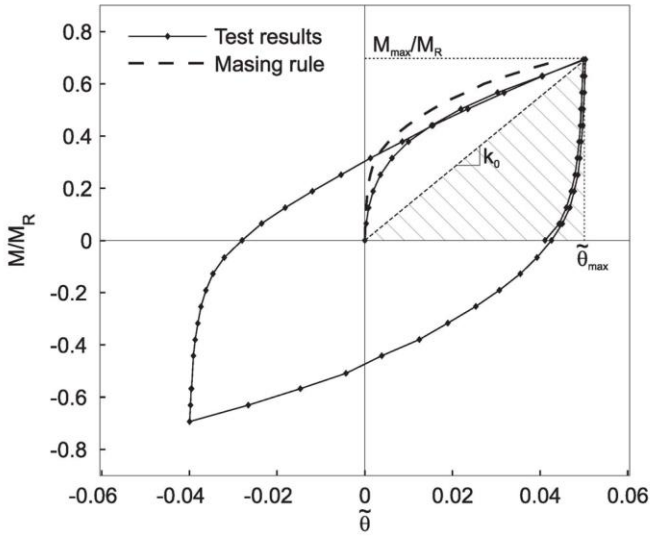

Fig6

Accepted manuscript doi:
10.1680/jgeot.16.p.325

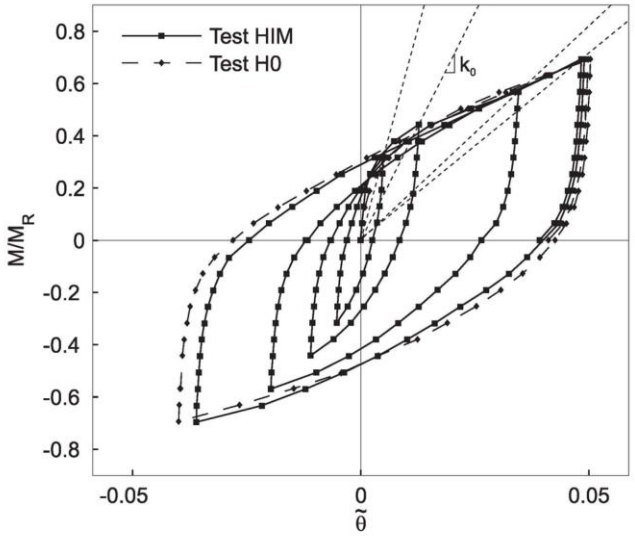

Fig7

Accepted manuscript doi:
10.1680/jgeot.16.p.325

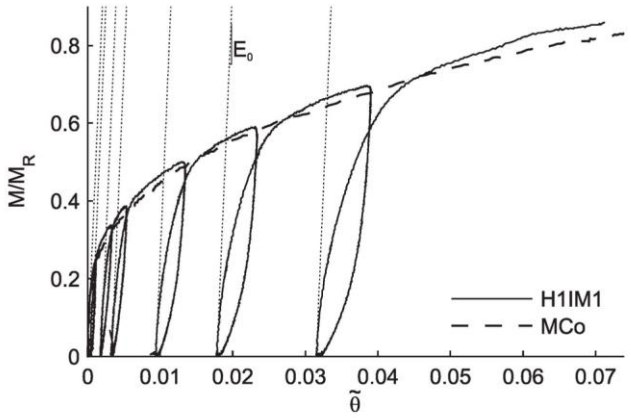

Fig8

Accepted manuscript doi:
10.1680/jgeot.16.p.325

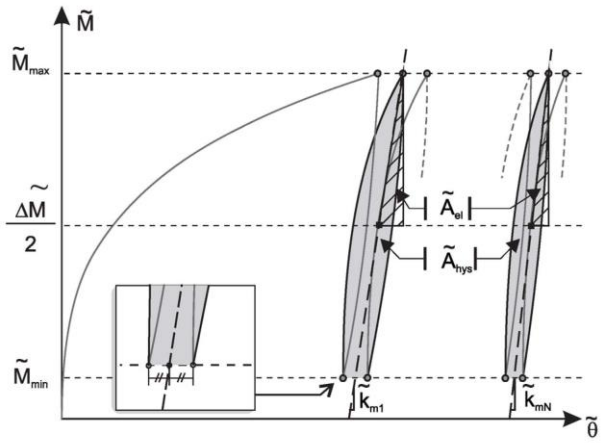

Fig9

Accepted manuscript doi:
10.1680/jgeot.16.p.325

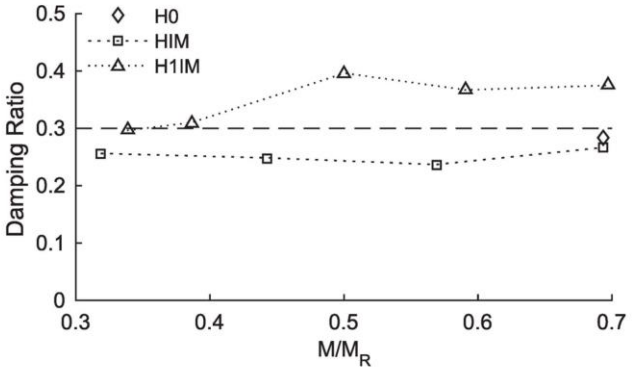

Fig10

Accepted manuscript doi:
10.1680/jgeot.16.p.325

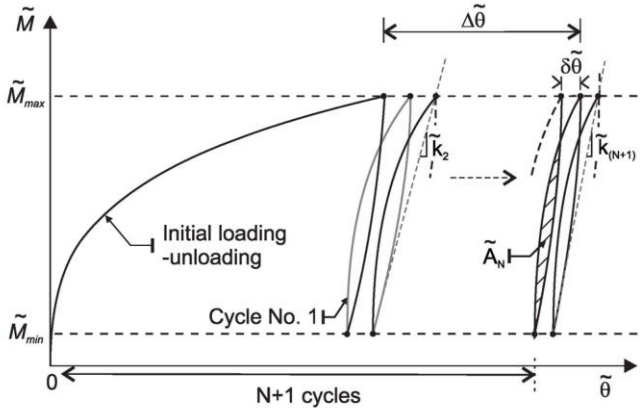

Fig11

Accepted manuscript doi:
10.1680/jgeot.16.p.325

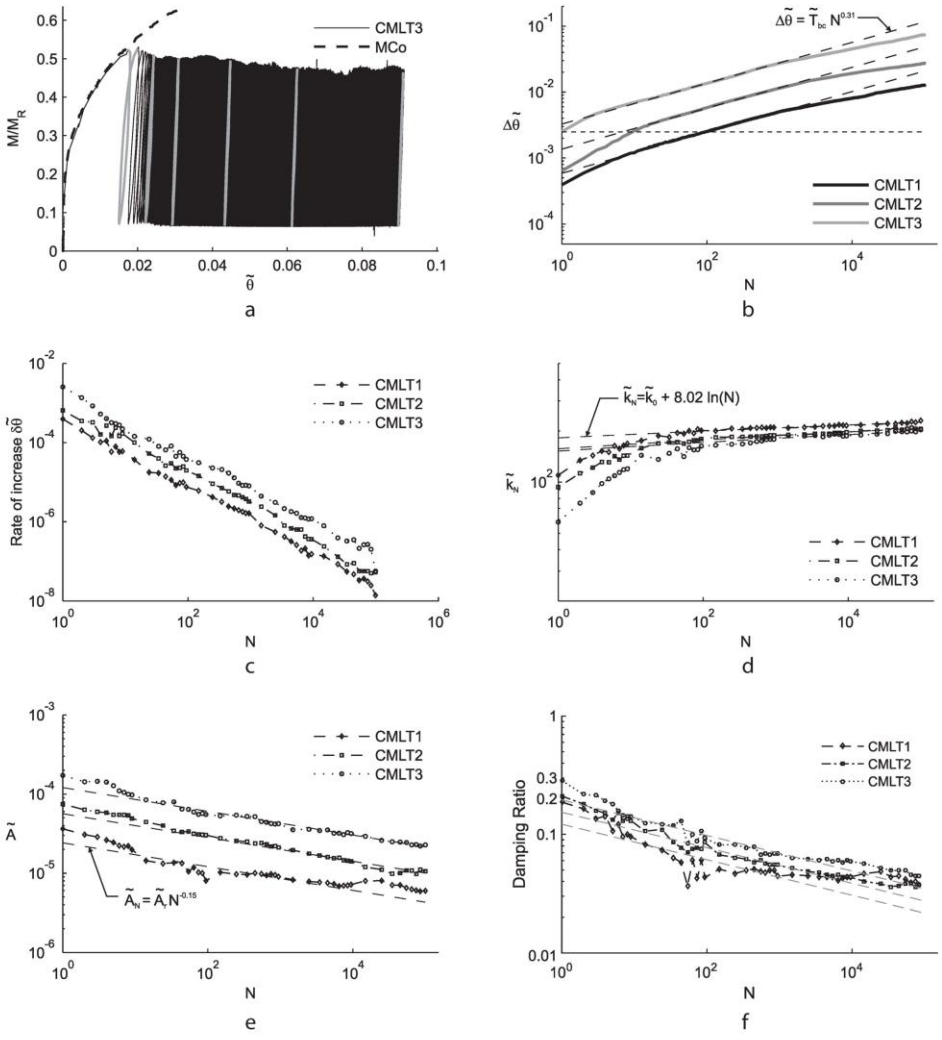

Fig12

Accepted manuscript doi:
10.1680/jgeot.16.p.325

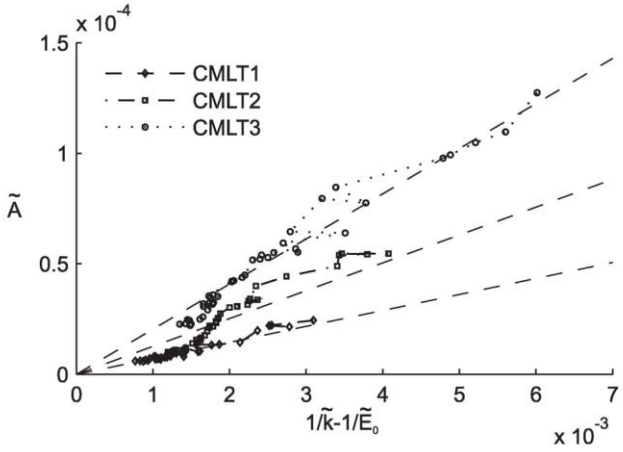

Fig13

Accepted manuscript doi:
10.1680/jgeot.16.p.325

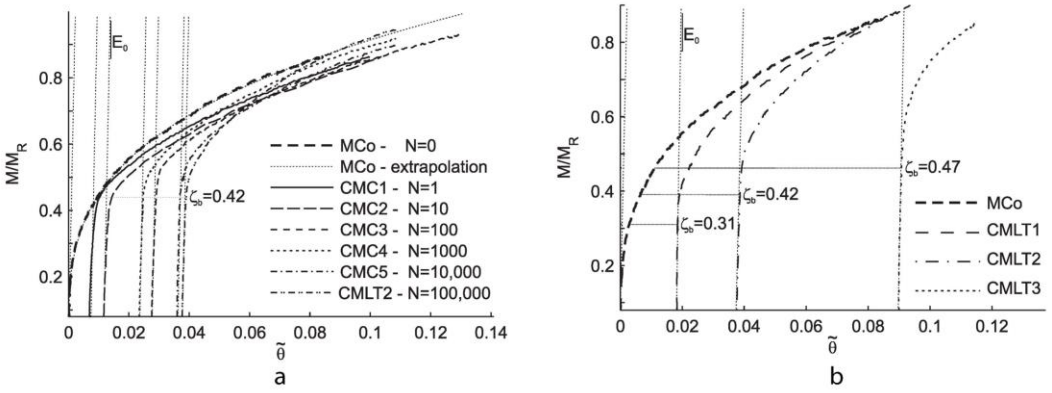

Fig14

Accepted manuscript doi:
10.1680/jgeot.16.p.325

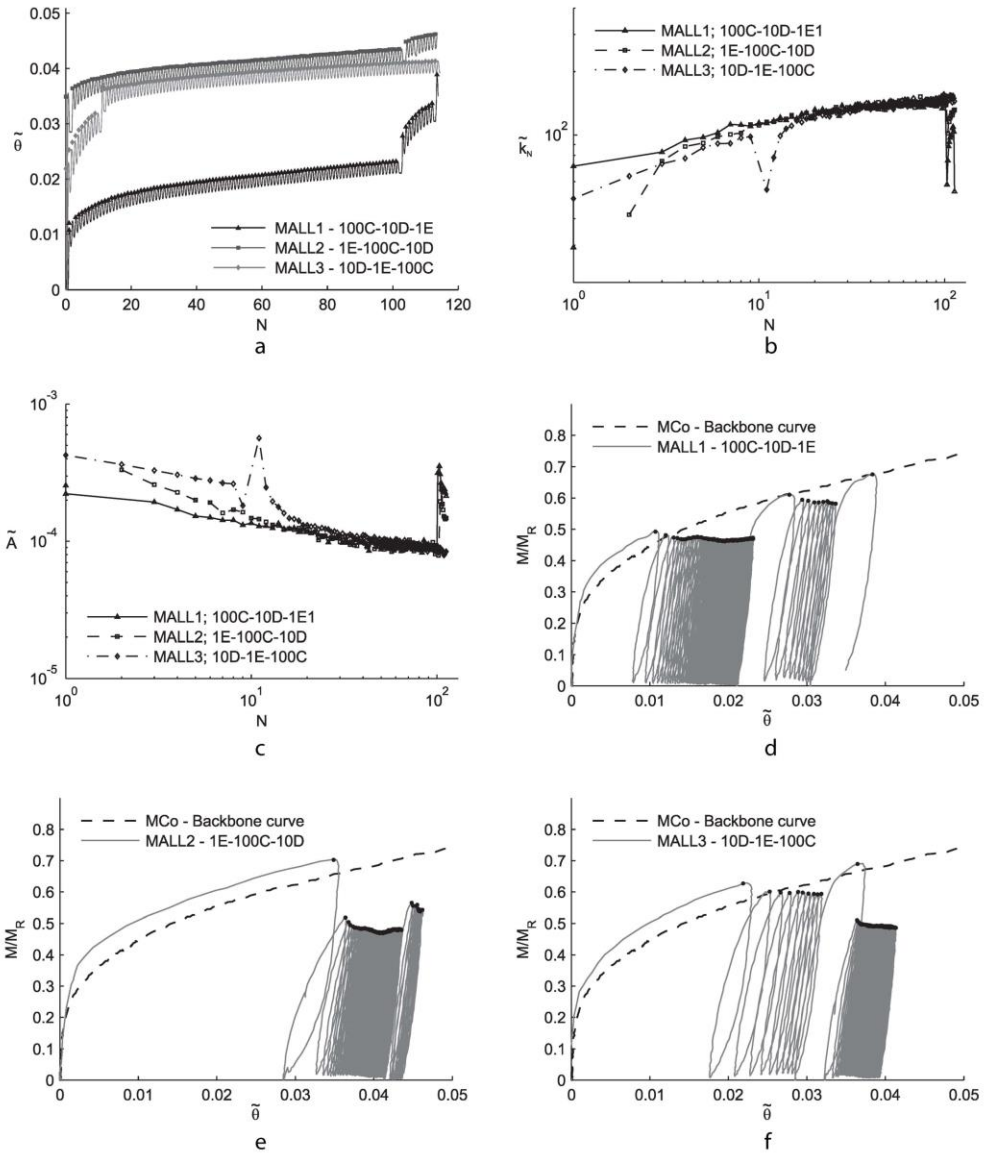

Fig15

Accepted manuscript doi:
10.1680/jgeot.16.p.325

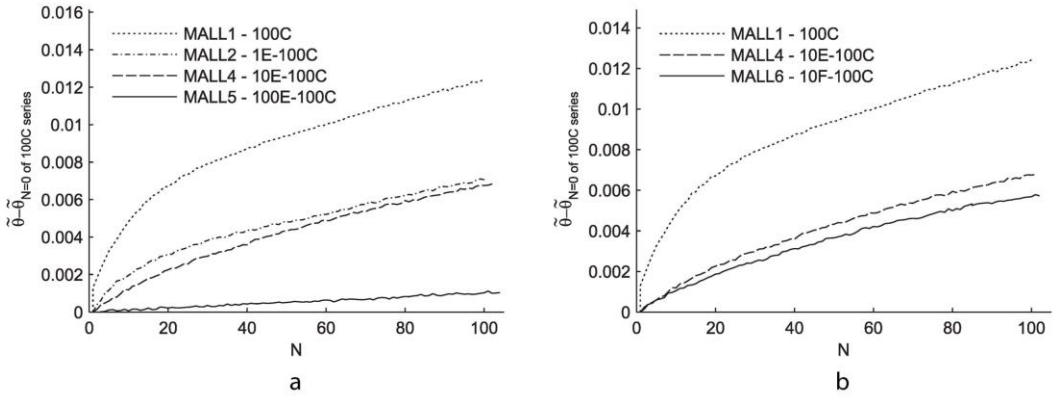

Fig16

Accepted manuscript doi:
10.1680/jgeot.16.p.325

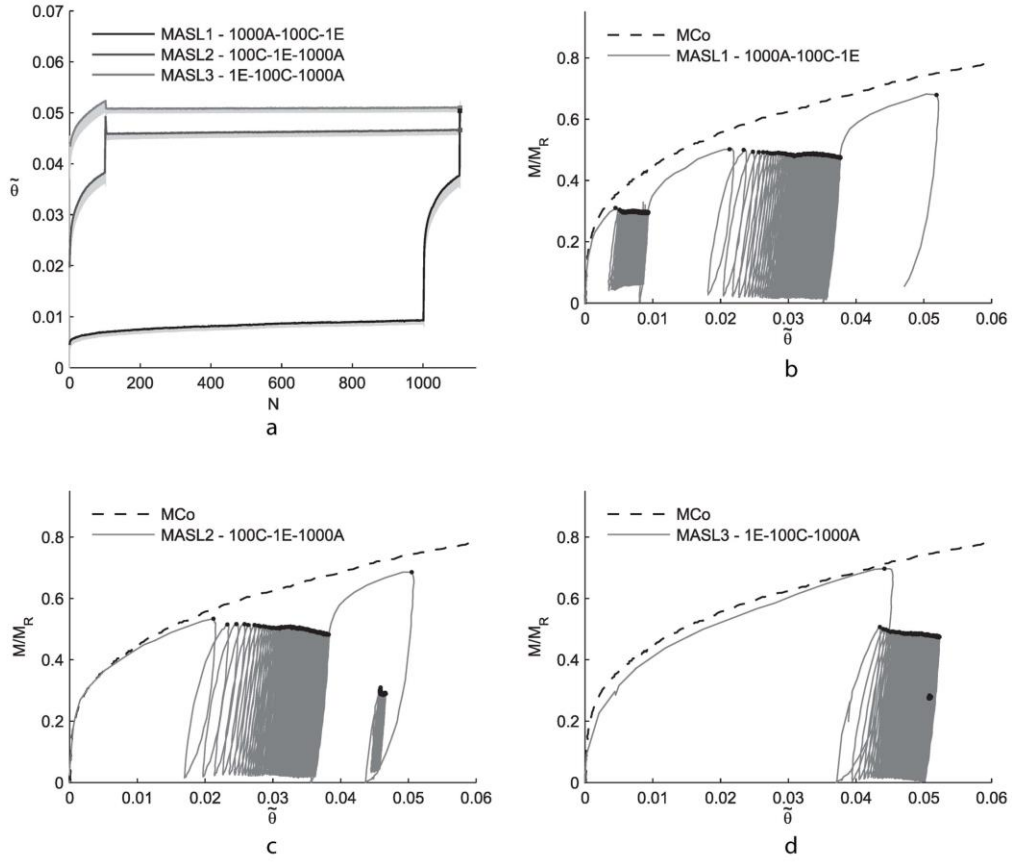

Fig17